

Article

Not peer-reviewed version

Lightweight Vivaldi Antenna for High-Voltage Ultra-Wideband Systems

[John J. Pantoja](#), [Omar A. Nova Manosalva](#)^{*}, [Hector F. Guarnizo Méndez](#), [Andrés Polochè Arango](#)

Posted Date: 30 January 2026

doi: 10.20944/preprints202601.2388.v1

Keywords: ultra-wideband; Vivaldi antenna; electromagnetic compatibility; ground-penetrating radar; hyperband antenna; impulse radiating antenna; electromagnetic interference; time-domain antenna







Preprints.org is a free multidisciplinary platform providing preprint service that is dedicated to making early versions of research outputs permanently available and citable. Preprints posted at Preprints.org appear in Web of Science, Crossref, Google Scholar, Scilit, Europe PMC.

Copyright: This open access article is published under a [Creative Commons CC BY 4.0 license](#), which permit the free download, distribution, and reuse, provided that the author and preprint are cited in any reuse.

Disclaimer/Publisher's Note: The statements, opinions, and data contained in all publications are solely those of the individual author(s) and contributor(s) and not of MDPI and/or the editor(s). MDPI and/or the editor(s) disclaim responsibility for any injury to people or property resulting from any ideas, methods, instructions, or products referred to in the content.

Article

Lightweight Vivaldi Antenna for High-Voltage Ultra-Wideband Systems

John J. Pantoja ¹, Omar A. Nova Manosalva ^{2,*}, Hector F. Guarnizo Méndez ³
and Andrés Polochè Arango ²

¹ Marshall Land Systems Ltd, The Airport, Newmarket Rd, Cambridge CB5 8RX, United Kingdom

² Electronics and Mechatronics Engineering Department, Fundación Universitaria Los Libertadores, Bogotá 111221, Colombia

³ Electronics Engineering Department, Universidad El Bosque, Bogotá 111321, Colombia

* Correspondence: oanovam@libertadores.edu.co

Abstract

This article presents the design and characterization process of a lightweight Vivaldi antenna for high-voltage ultra-wideband systems. The proposed antenna consists of two radiating arms with different exponential curves on their inner and outer edges fed with an insulated-coplanar-plates transmission line. The weight reduction is achieved by implementing the antenna with sheets composed of a polyester layer between two aluminum layers, with a polylactic acid insulator inserted between the arms. The reflection coefficient of the implemented antenna demonstrates an impedance bandwidth ranging from 0.3 GHz to 4.2 GHz. High voltage operation of up to 12.4 kV is also experimentally demonstrated. The transfer function between the voltage applied to the antenna, V_s , and the radiated electric field, E_r , is measured. Using this transfer function, the radiated electric field is calculated for an input voltage pulse with a rise time of 110 ps to confirm the antenna capability of producing radiated pulses with low distortion. The calculated radiated electric field pulse closely matches the results obtained with full wave simulation. To assess the similarity between the radiated and applied pulses, the pulse width stretch ratio is calculated, yielding a variation of 3.86% for the direction of maximum gain and 9.36% for 30° in the H-plane of the antenna. This feature is desirable for EMC, EMI and sensing applications. The antenna is also characterized in the frequency domain, achieving a maximum gain of 13.9 dBi at 3 GHz and a 30° 3dB beamwidth for ultra-wideband pulses.

Keywords: ultra-wideband; Vivaldi antenna; electromagnetic compatibility; ground-penetrating radar; hyperband antenna; impulse radiating antenna; electromagnetic interference; time-domain antenna

1. Introduction

Ultra-wideband (UWB) antennas are key enabling components of modern wireless technologies that require high speed [1], high bandwidth [2], diversity [3,4], and low signal distortion [5]. Applications range from high-speed data transmission [6], water detection [7], landmine detection [8], to biomedical imaging [9,10], radar [11], through-wall radar (TWR) [12], fluid properties determination [13], and intentional electromagnetic interference [14], as shown in Figure 1. One of the most widely used antennas for UWB applications is the Vivaldi antenna, a type of tapered slot antenna (TSA). Originally called Vivaldi aerial [15], the Vivaldi antenna is characterized by its high gain, wide bandwidth, low cross-polarization level, and stable radiation characteristics. Various optimization techniques have been proposed to enhance its performance, including feeding mechanisms, slot integration, radiator shape modifications, inclusion of dielectric lenses, parasitic patches between the two radiator arms, edge corrugations on the arms, and the use of metamaterials [16].

Vivaldi antennas are commonly used in ground-penetrating radar (GPR) due to the characteristics mentioned above and also due to their compactness [17]. GPR antennas must meet the following conditions: they must be broadband, have narrow beam-width radiation patterns, and be capable of

radiating medium-power pulses. In the case of bi-static GPR, low crosstalk is also required. Crosstalk can be reduced by using arrays with directive antennas, such as Vivaldi [18,19] and shielded bowtie [20] antennas. Besides, it is necessary to consider the near-field interaction with the soil and the target, which affects crosstalk, impedance matching, and detection efficiency. Stadler et al. [21] show that full-wave simulation approach including the antenna model is required to accurately determine the near-field antenna coupling with the soil, which has frequency dependent permittivity in the GPR operational frequency range [22].

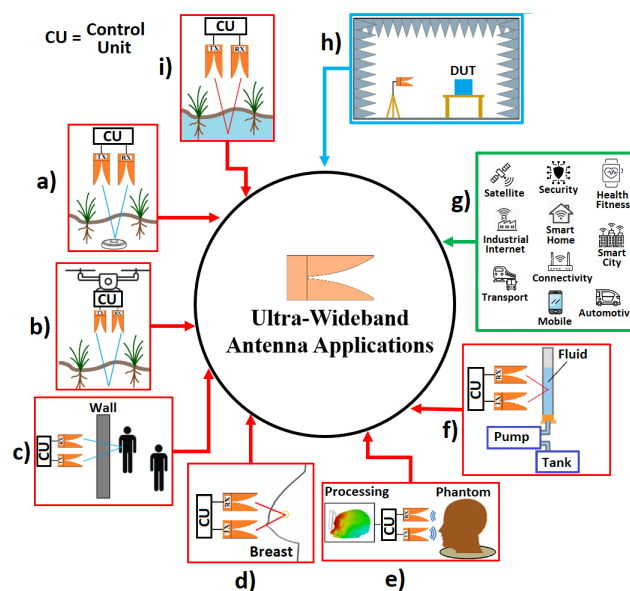


Figure 1. Ultra-Wideband Antenna Applications, a) Detecting Buried Objects, b) Airborne GPR, c) Through-Wall Radar, d) Microwave Tomography, e) Microwave Imaging, f) Fluids Characterization, g) Wideband Communications, h) IEMI or EMC and i) Water Detection.

To achieve broadband performance, geometries such as the hybrid antenna presented in [23] can be used. This design combines two modes of operation: a broadband monopole mode between 200 MHz and 400 MHz, and a Vivaldi antenna mode between 400 MHz and 25 GHz. In this case, the radiation pattern is not critical, as the antenna is designed to be used in a reverberation chamber (RC), where mode stirrers generate an isotropic average antenna pattern.

UWB antennas are also used to characterize radiated pulsed emanations of secure communications systems [24]. Typical spectral content of radiated signals from components used in quantum communications, for instance, ranges from 40 MHz to 1 GHz [25]. UWB directive antennas, such as double-ridge guide horn, are preferred for electromagnetic (EM) emission measurements. However, to achieve low frequency operation, size and weight scale up resulting in large (i.e. squared meter aperture or cross-section) and heavy (i.e. tens of kg) antennas [26].

UWB antennas for electromagnetic compatibility (EMC) tests must have stable characteristics with frequency. In [27], the development of a Vivaldi antenna for electromagnetic field measurements in EMC tests between 0.5 GHz and 4 GHz is presented. This antenna is a low-cost alternative compared to other options covering the same frequency range and allows the replacement of multiple narrowband antennas traditionally used for these tests.

Directive antennas are preferred for radiated immunity and intentional electromagnetic interference (IEMI) testing. These tests require compliance with field uniformity criteria on surfaces where the devices under test (DUT) are located. A hyperband antenna for IEMI applications is presented in [28]. In addition to achieving the field uniformity criterion, this antenna achieves the radiation of high-power pulses with amplitudes on the order of 6 kV. The bandwidth of this antenna is also wide, as it can radiate pulses with a rise time on the order of 90 ps. Recently, tests have been reported on this antenna with source voltages up to 24 kV [29].

One option to achieve radiation patterns with high gain and beam-steering capability is through the use of antenna arrays. An example of such an array, with broadband operation, is presented in [30]. This array is capable of radiating high power for use in high-power jamming systems. To prevent arc flashes when handling high power, the antenna tips are rounded to reduce the electric field intensity around them. Additionally, the array is constructed entirely of metal, as antennas manufactured on substrates tend to have low durability when operated at high power. An 8x8 array with a $\pm 45^\circ$ slant configuration operates between 2 GHz and 6 GHz, achieving gains between 18 dBi and 21 dBi for various beam-steering angles.

In [31], a linear 1x10 array of antipodal Vivaldi antennas is presented, where the effect of adding metallic inserts to the metallizations and slots of each element is explored. The best performance is observed when two inserts are added to the slots, resulting in an operating frequency range from 5.7 GHz to 12.0 GHz, a gain between 12 dBi and 19 dBi within this range, and a radiated power between 0.75 W and 0.9 W.

In [32], a compact Vivaldi antenna array for UWB pulse radiation is proposed. To compact the array, the ends of the radiating elements are bent in both directions. To expand the impedance bandwidth, short-circuited branches are inserted between the bent radiating elements and the ground plane. This design results in an 8x4 array capable of radiating UWB pulses with an impedance bandwidth ranging from 0.6 GHz to 6 GHz, and a compact size of 2.5 cm x 2.5 cm x 4.5 cm. The gain varies between 5 dBi and 20 dBi.

Antennas capable of radiating pulses must be analyzed not only in the frequency domain but also in the time domain. While parameters such as gain, reflection coefficient, and group delay as a function of frequency are important, they are insufficient for this type of antenna. It is necessary to characterize the distortion introduced by the antenna on the transmitted pulses [33]. This time-domain characterization includes parameters such as pulse width extension and fidelity factor to establish the similarity between the transmitted and received pulses [34].

A common application of antennas capable of radiating high-power pulses is through-wall radar and imaging of nearby objects. For through-wall radar (TWR), antennas with high gain, wide bandwidth, and effective wall penetration capabilities are required. These features are provided by the Vivaldi antenna, which also exhibits directional radiation patterns that enhance wall penetration. In [35], structural optimizations, feeding techniques, and performance improvement strategies for Vivaldi antennas are presented to enhance their imaging and detection capabilities for through-wall radar applications.

For imaging nearby objects, [36] describes the design of an antipodal Vivaldi antenna (AVA) capable of radiating impulse-type waveforms. The antenna operates between 1.8 GHz and 10 GHz, and its design focuses on optimizing its pulse response in the time domain. This involves analyzing the transfer function between two identical antennas, the shape of the received pulse, group delay, and gain. The antenna successfully reconstructs two radar targets positioned 7 cm apart.

A comparison of the relevant parameters for various UWB antennas for EMC, IEMI, and radar applications is presented in Table 1. The table shows that the starting operation frequency of the UWB antennas is higher than 0.5 GHz for most of the cases, even though the applications may require to cover lower frequencies. This is due to size and weight constraints. To overcome this problem, in this paper, we propose a lightweight UWB differential antenna with a starting frequency of 0.33 GHz suitable for GPR, EMC, and EMI applications. The antenna presented here is optimized for wide-band impedance matching up to 4.2 GHz. The frequency domain and also the time domain performances are analyzed in detail.

This paper is organized as follows. Section II outlines the antenna design to achieve the desired impedance matching. Section III describes the procedure for implementing and testing the antenna, presenting the obtained reflection coefficient and the radiated electric field. Section IV details the characterization of the designed antenna in the time domain, presenting an analysis of the waveform

responses and calculating the pulse width stretch ratio (SR) for different pulses over the main planes of the antenna.

Figure 2 summarizes the workflow followed in this study: (i) geometry definition and Ansys HFSS-based parametric design of a differential Vivaldi with exponential inner/outer tapers and a PLA spacer, using lightweight aluminum–polyester–aluminum sheets; (ii) prototype fabrication and high-voltage feed implementation with ferrite-ring and tapered-coax baluns, qualified to 12.4 kV; (iii) frequency-domain validation with a VNA showing a measured impedance bandwidth of 335.8 MHz–4.2 GHz; and (iv) time-domain assessment using a 110 ps input pulse and an S_{21} -derived transfer function to compute the radiated field $E_r(t)$, followed by pulse-fidelity analysis—pulse-width stretch ratio $< 10\%$ up to $\pm 30^\circ$ —and a $\sim 30^\circ$ 3 dB beamwidth for UWB pulses. This process map clarifies how the lightweight, wideband, and high-voltage requirements were achieved and verified.

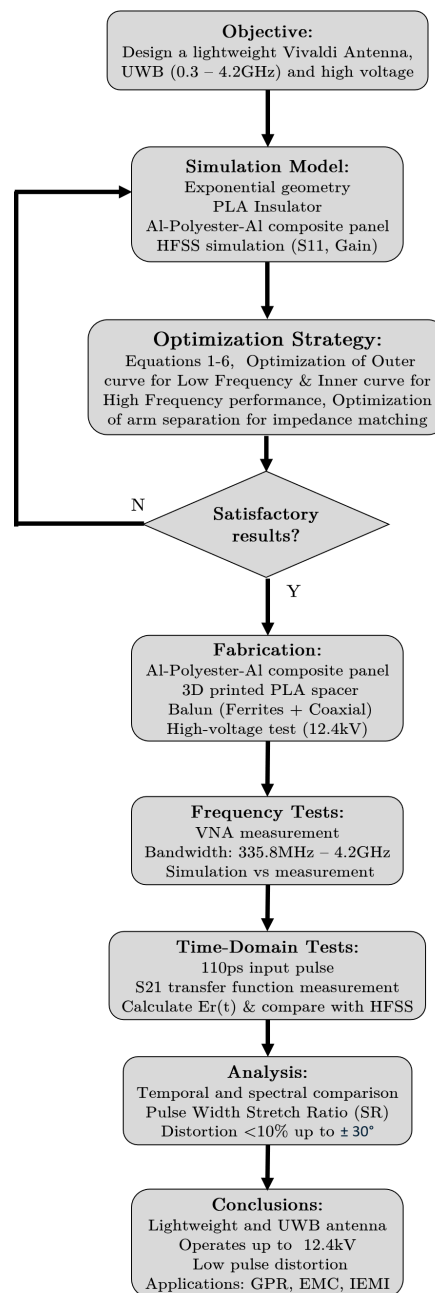


Figure 2. Workflow followed in this study.

Table 1. Comparison of UWB antennas for EMC, IEMI and radar applications.

Description	Application	Freq. Band (GHz)	Bandwidth (GHz)	Gain (dBi)	Max. Voltage / Power	Ref.
Hybrid Monopole/Vivaldi	EMC	0.2 - 25	24.8	–	–	[23,29]
Hyperband Vivaldi	IEMI	–	3*	–	34 kV	[28]
UWB 10-element Vivaldi array	–	5.7 - 12	6.3	11 - 20	0.9 W	[31]
Compact Vivaldi array	UWB pulse system	0.6 - 6	5.4	5 - 20	100 kV	[32]
Vivaldi for EMC	EMC	0.5 - 4	3.5	0 - 6.5	–	[27]
Vivaldi for radar	TWR	1.8 - 10	8.2	0 - 10	–	[36]
Broadband TEM Horn Antenna	EMI	0.38 - 6	5.62	2 - 10	300 W	[37]
Proposed design	GPR, EMC	0.33 - 4.2	3.87	0 - 13.88	12.4 kV	–

* Estimated from 90 ps rise time.

2. Antenna Design

Various design approaches have been proposed to improve the performance of Vivaldi antennas in ground-penetrating radar (GPR) applications. These include the incorporation of combined slots at the edges to extend the electrical length and achieve frequencies from 75 MHz [38], the optimization of feeding strategies such as microstrip, curved microstrip, and CPW to expand bandwidth and gain [39], the inclusion of elliptical slots in antipodal E-shaped configurations to reduce the cutoff frequency [40], and the design of S-band Vivaldi arrays optimized by parametric sweeps to improve coupling and directivity [41].

Various antenna configurations have been proposed to improve the performance of GPR systems. These include a suspended elliptical patch with an optimized slot that achieves bandwidths of 878–1260 MHz and gain >8 dBi [42]; a low-profile bowtie antenna with a loaded elliptical patch and reflector plane, which reduces the minimum frequency to 0.18 GHz and achieves compact dimensions with 7.41 dBi gain [43]; and a slotted bowtie with bent arms and absorbent backing, covering 0.5–3 GHz and offering >30 dB isolation [44].

UWB antennas such as the one designed in this article can also be used in applications that require high-capacity, low-latency and reliable communications in 5G/6G networks [45], as well as in satellite links using MIMO-UWB systems, which increase spectral efficiency and support emerging applications such as IoT and massive communications [46].

In electromagnetic compatibility tests, antennas are made to withstand high voltages through the use of multilayer lenses that adjust dielectric constants and improve directivity [47], and geometric optimization of the aperture and propagation in TEM horn antennas [48].

Three main goals are addressed in the design using novel optimization and fabrication techniques: (i) wide-band impedance matching by optimizing the geometry and materials through parametric simulations, (ii) light weight by using aluminum composite boards, and (iii) high voltage by isolating the differential feed point.

2.1. Geometry and Materials

The configuration of the proposed Vivaldi antenna is shown in Figure 3. This antenna is designed from two identical conductive arms (radiating arms) with an insulator of polylactic acid (PLA) between

the arms. The material of the radiating arms is aluminum. The antenna size is set at 64.2 (x_1) x 48 (y_1) cm².

The inner curves of the antenna (see Figure 3) follow an exponential function described by:

$$y = F_1 e^{Mx} + F_2 \quad (1)$$

where,

$$F_1 = \frac{(y_d - y_b)}{(e^{Mx_c} - e^{Mx_a})} \quad (2)$$

$$F_2 = \frac{(y_b e^{Mx_a} - y_d e^{Mx_c})}{(e^{Mx_c} - e^{Mx_a})} \quad (3)$$

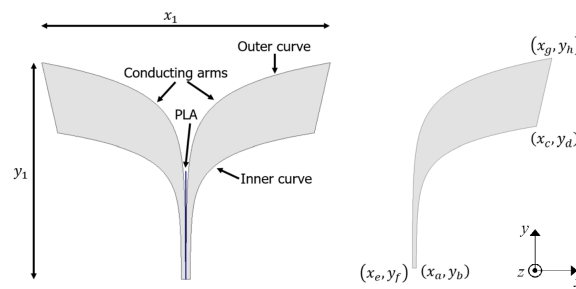


Figure 3. Proposed Vivaldi antenna.

The outer curves of the antenna (see Figure 3) follow an exponential function described by:

$$y_D = E_1 e^{Nx} + E_2 \quad (4)$$

where,

$$E_1 = \frac{(y_h - y_f)}{(e^{Nx_g} - e^{Nx_e})} \quad (5)$$

$$E_2 = \frac{(y_f e^{Nx_e} - y_h e^{Nx_g})}{(e^{Nx_g} - e^{Nx_e})} \quad (6)$$

The equations symbols are presented in Table 2 and Figure 3. The values of these symbols are given in Table 3.

Equations 1 - 6 were used to obtain an initial state for the antenna. Parametric analysis was then used in Ansys HFSS to maximize bandwidth. This analysis included optimization of the outer curve for low frequency performance, optimization of the inner curve for high frequency performance, and optimization of arm separation for impedance matching.

Table 2. Symbols for the equations of the inner and outer curves of the antenna.

Symbol	Representation
(x_a, y_b)	Starting point of the inner curve
(x_c, y_d)	End point of the inner curve
M	Curvature rate of the inner curve
(x_e, y_f)	Starting point of the outer curve
(x_g, y_h)	End point of the outer curve
N	Curvature rate of the outer curve

Table 3. Dimensions of the proposed Vivaldi antenna.

Parameter	Value (mm)	Parameter	Value (mm)
x_1	642	z_1	3
x_2	571	z_2	6
x_3	9	y_1	480
x_4	9	y_2	324
x_5	20	y_3	240
x_a	10	y_b	0
x_c	285	y_d	324
x_e	1	y_f	0
x_g	321	y_h	480

2.2. Weight Reduction

To reduce the overall weight of the antenna, each conductive arm was replaced by a layered structure with one dielectric layer of 2 mm in between two conductive layers of 0.5 mm. That is, from bottom to top there is a conductive layer (aluminum), then a second dielectric layer (polyester) and finally a third conductive layer (aluminum). Using aluminum composite panels provides a weight reduction of 66.7% when compared to same-size aluminum sheet. Figure 4 shows the final configuration of the proposed Vivaldi antenna. The simulation was conducted using Ansys HFSS, where the dimensions of the radiation box were adjusted to $14.5 \times 14.5 \times 14.5 \text{ cm}^3$.

Table 3 shows the parameters and their values for the proposed antenna. Figure 5 shows the S_{11} parameter of the proposed antenna with and without insulator (i.e. PLA). It is observed that the antenna matching improves with the presence of the insulator located between the conductive arms.

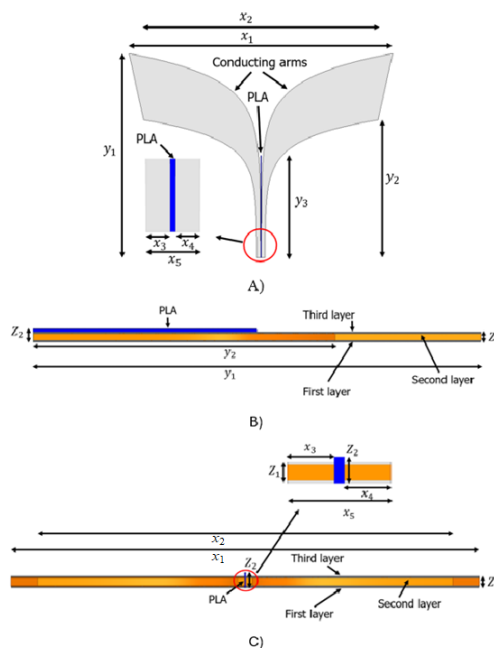


Figure 4. Final configuration of the proposed Vivaldi antenna, A) top view, B) side view, C) front view.

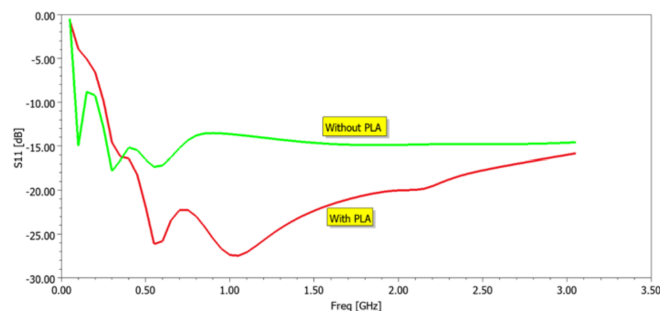


Figure 5. Comparison of the simulated reflection coefficient of the antenna with and without PLA insulator between the arms.

2.3. Feed Point

The antenna feed point was designed to handle high voltage and provide a wideband transition to a single-ended coaxial transmission line. In addition to improve the matching impedance, the PLA strip between the two arms also provides electric insulation. It was experimentally verified that the design has a breakdown voltage of 12.4 kV. Figure 6 shows a spark produced during the test when the high voltage applied at the feed point exceeds this threshold. A balun was implemented using two ferrite rings of 4W620 material from Würth Elektronik on the differential transmission line at the feed point. This provides common-mode current rejection up to 1 GHz. To provide a smooth transition for higher frequencies, a coaxial cable tapered balun was implemented at the connection point by gradually removing the screen of the coaxial cable.

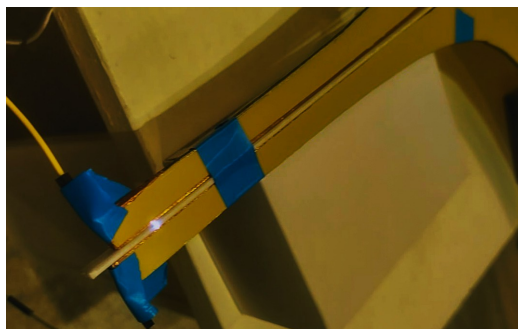


Figure 6. High-voltage test of the antenna feed point. A spark is produced around the PLA insulator at 12.4 kV.

2.4. Gain

The maximum gain of the main lobe of the designed Vivaldi antenna was simulated in Ansys HFSS, with the results shown in Figure 7. The gain varies between -7.66 dBi and 13.88 dBi over a frequency range of 0.1 GHz to 3 GHz. The gain is positive throughout the frequency range from 0.15 GHz to 3 GHz, except for a negative gain point of -1.09 dBi at 0.65 GHz. This negative gain point coincides with a region of antenna mismatch (see Figure 11). The antenna exhibits peak gain values at frequencies of 0.25, 0.5, 0.95, 2.3, and 3 GHz, achieving gains of 6.72, 7.61, 6.24, 10.87, and 13.88 dBi, respectively.

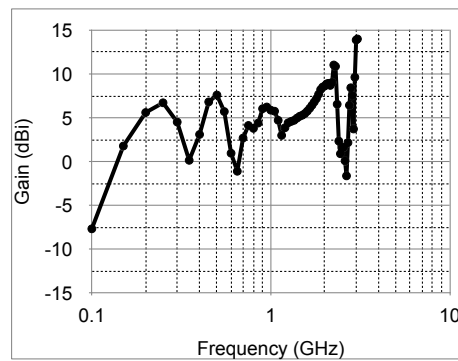


Figure 7. Maximum gain of the proposed Vivaldi antenna.

2.5. Radiation Patterns

The normalized gain radiation patterns of the antenna are plotted in the E-plane (xy-plane in Figure 3) and H-plane (yz-plane in Figure 3), as shown in Figure 8 and Figure 9, respectively, at frequencies distributed throughout the antenna's matching range. The radiation patterns show uniformity in their shape in the two main planes, although as the frequency increases, more secondary lobes appear. The radiation patterns presented confirm the uniformity of the maximum gain as a function of frequency.

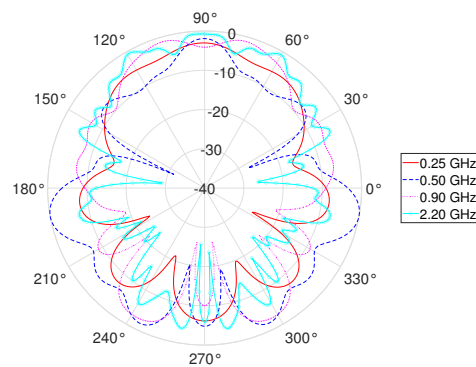


Figure 8. Normalized gain radiation patterns in the E-plane.

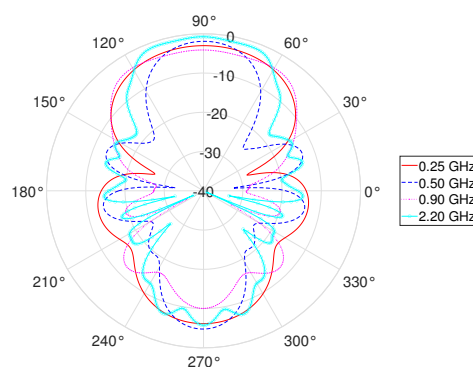


Figure 9. Normalized gain radiation patterns in the H-plane.

3. Antenna Testing

The proposed Vivaldi antenna was fabricated and measured as shown in Figure 10. The arms were implemented with a sheet composed by two layers of aluminium filled with polyester composite. The layered sheet provides the required strength for the arms size and light weight. Total weight of the antenna is less than 600 g. A 3D printed PLA insulator between the arms was added to adjust the matching impedance. The insulator also enables the antenna to operate at high voltages as discussed before.

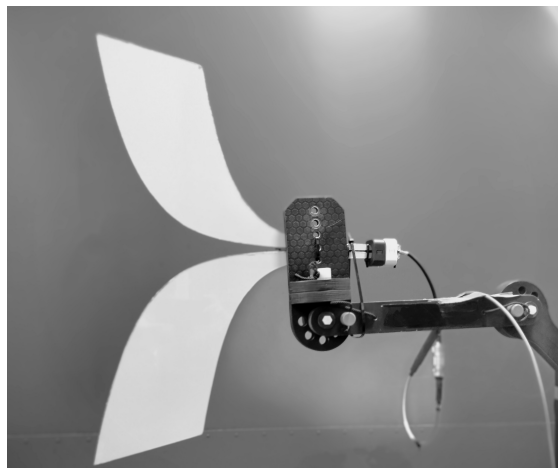


Figure 10. Ultra-wideband antenna and wooden support attached to testing mast.

The measurement was conducted using a portable network vector analyzer. Figure 11 shows the measured reflection coefficient of the Vivaldi antenna. The impedance bandwidth obtained from the measurements is 335.8 MHz to 4.2 GHz. A slight mismatch is presented at 600 MHz. This small discrepancy between simulated and measured results are due to the inclusion of elements added during the fabrication, which were neglected in the simulation, such as the ferrites and the wooden support.

This impedance bandwidth corresponds to a fractional bandwidth of 1.70, classifying the antenna as an ultra-wideband (UWB) device for radar and communication applications, and as a hyperband (HB) device for electromagnetic interference applications [49].

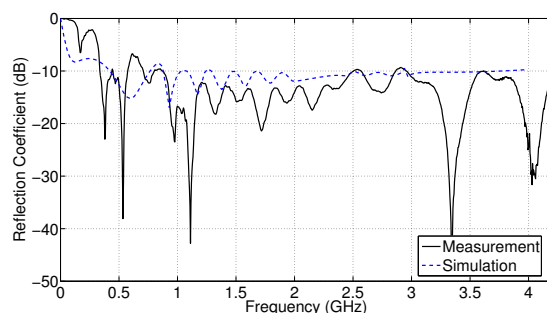


Figure 11. Input reflection coefficient of the implemented antenna.

3.1. Radiated Electric Field Measurement

The electric field radiated by the Vivaldi antenna was measured using a reference biconical antenna as shown Figure 12. Both antennas were $h = 1.5$ m high and separated by a distance $d = 2.9$ m. The S-parameters between the reference antenna and the antenna under test were measured as presented in the diagram of Figure 13 to obtain the transfer function between the incident voltage wave at port 2, b_2 , and the reflected wave at port 1, a_1 . That relationship, shown in (7), is the voltage forward gain (VFG). In our measurement, VFG is the ratio between the received voltage, V_r , and the voltage applied to the Vivaldi antenna, V_s , in the frequency range where both antennas are impedance matched.

$$S_{21} = \frac{b_2}{a_1} \quad (7)$$

To calculate the radiated electric field E_r , the antenna factor of the receiving antenna AF can be used as shown in (8).

$$AF = \frac{E_r}{V_r} \quad (8)$$

Using (7), (8), and replacing a_1 and b_2 by V_s and V_r , respectively, the radiated electric field can be calculated as

$$E_r = AF \cdot S_{21} \cdot V_s \quad (9)$$

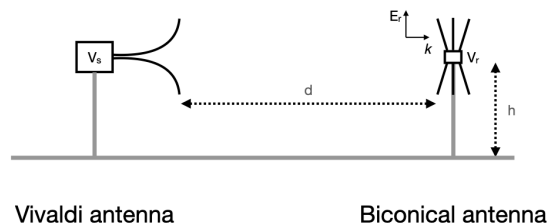


Figure 12. Measurement setup of the antenna radiated electric field.

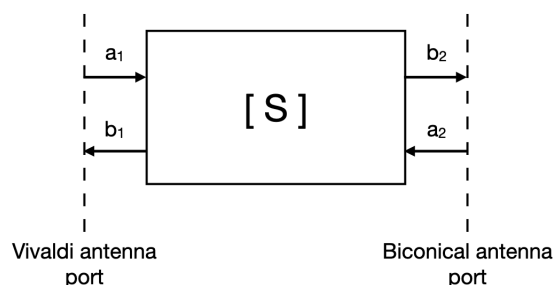


Figure 13. Diagram of the S-parameters two-port measurement performed to obtain the transfer function of the Vivaldi antenna.

Figure 14 shows the electric field radiated by the Vivaldi antenna scaled to 1 m in vertical polarization. 6 measurements were conducted and normalized to 1 m. The figure shows a wide-band frequency response with a resonant transfer function between 0.15 and 3 GHz.

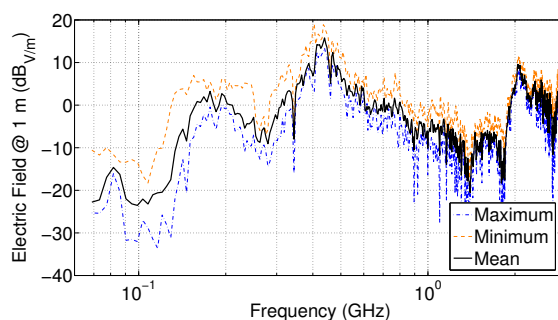


Figure 14. Received electric field scaled to 1 m and normalized to 1 V at the antenna port. Mean, maximum, and minimum values of 6 tests.

4. Time-Domain Characteristics

4.1. Waveform Responses

To obtain the received electric field E_r for an input signal corresponding to a wideband pulse, in (9) V_s is replaced by the pulse shown in Figure 15, whose rise time is 110 ps.

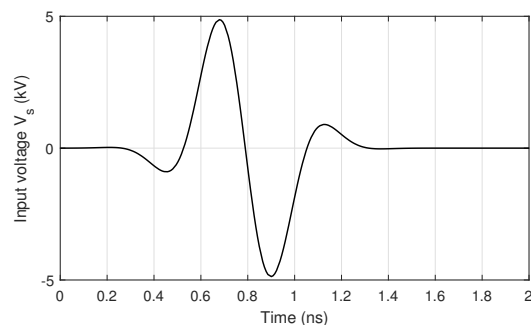


Figure 15. Pulse V_s applied to the Vivaldi antenna input.

The frequency spectrum obtained for E_r is converted to the time domain using the inverse Fourier transform, resulting in the measured pulse presented in Figure 16. The received pulse corresponds to the electric field scaled to 1 m. The figure shows the comparison of the calculated signal and the simulated pulse from Ansys HFSS, obtained as the parameter rE .

In Figure 16 good agreement is observed in the shape and width of the simulated and measured pulses with small differences in the amplitude and width of the two positive peaks. This figure shows that the radiated electric field waveform is the derivative of the applied voltage typically produced by the Vivaldi antenna [14,50].

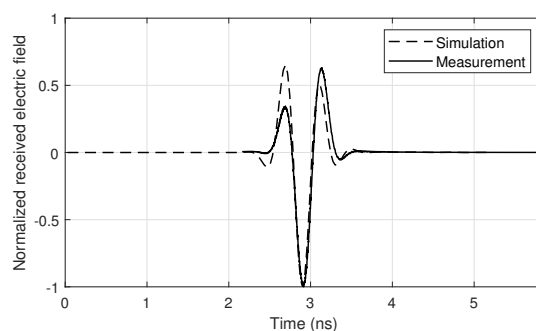


Figure 16. Received electric field pulses E_r scaled to 1 m and normalized to 1 V/m.

To determine the similarity between the received and the input pulses, they are compared in the frequency domain (Figure 17). The frequency spectra are obtained through the Fourier transform of the pulses. A comparison of the spectra shows that they are centered around the same frequency (1.875 GHz). Despite minor amplitude differences, the spectra satisfactorily include signals within the range of 0.5 GHz to 3.5 GHz.

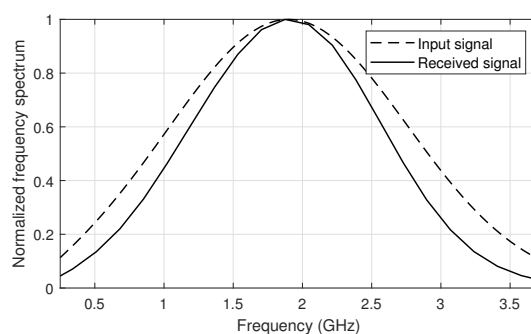


Figure 17. Frequency spectra of the input and received signals.

4.2. Pulse Width Stretch Ratio (SR)

To analyze how the received pulses stretch compared to the input pulse, the parameter pulse width stretch ratio (SR) is used, as defined in (10) and (11) [33,51].

$$E_s(t) = \frac{\int_{-\infty}^t |s(t')|^2 dt'}{\int_{-\infty}^{\infty} |s(t')|^2 dt'} \quad (10)$$

$$SR = \frac{E_{s2}^{-1}(0.95) - E_{s2}^{-1}(0.05)}{E_{s1}^{-1}(0.95) - E_{s1}^{-1}(0.05)} \quad (11)$$

In the numerator of (11), the width of the pulse of interest (signal s_2) is calculated as the time interval between the times where the accumulated pulse energy reaches 5% and 95% of its total energy. This width is compared to that of a reference signal (signal s_1), calculated in the same manner, in the denominator of (11).

In this case, the pulses of interest, s_2 , correspond to the electric field scaled to a distance of 1 m on the main lobe of the antenna, in both the E-plane and H-plane, at angles of 0° (maximum radiation direction), 15° , 30° , -15° , and -30° . These pulses are shown in Figure 18 and Figure 19.

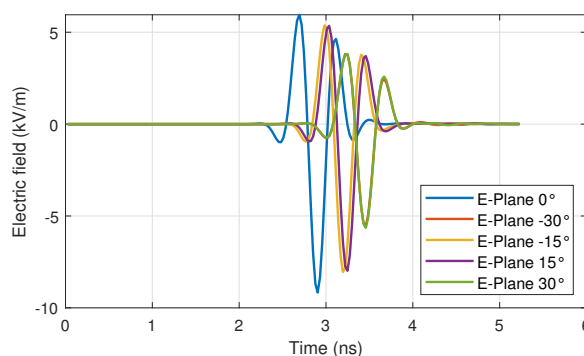


Figure 18. Electric field pulses scaled to 1 m on the E-plane of the antenna's main lobe.

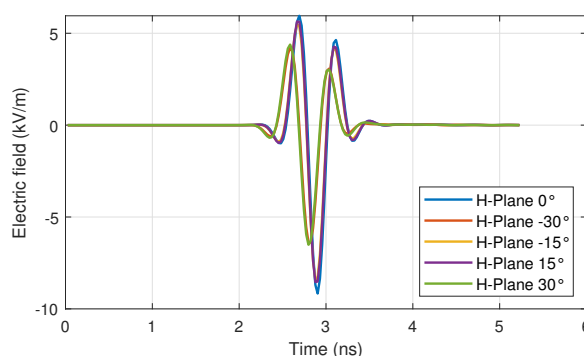


Figure 19. Electric field pulses scaled to 1 m on the H-plane of the antenna's main lobe.

Two pulses were used as reference signal s_1 in (11): the input voltage V_s , shown in Figure 15, and its derivative. The derivative was used because, as previously mentioned, in a pulse-radiating antenna, the radiated electric field has the form of the derivative of the input voltage [14,50]. Since the pulses of interest s_2 are radiated electric fields, it is appropriate to use the derivative of the voltage as a reference. The input voltage itself is also used as a reference to evaluate the stretching of the radiated pulses relative to the driving signal. The pulse width stretch ratio (SR) calculated for the two reference signals s_1 is presented in Table 4 and Table 5.

Table 4. SR using V_s as the reference pulse.

Plane	SR for different angles on the principal planes				
	-30°	-15°	0°	15°	30°
E-Plane	1.3703	1.3420	1.3350	1.3420	1.3703
H-Plane	1.3844	1.3420	1.3350	1.3491	1.4056

Table 5. SR using $\frac{dV_s}{dt}$ as the reference pulse.

Plane	SR for different angles on the principal planes				
	-30°	-15°	0°	15°	30°
E-Plane	1.0661	1.0441	1.0386	1.0441	1.0661
H-Plane	1.0771	1.0441	1.0386	1.0496	1.0936

As expected, the SR value is closer to 1.0 when the derivative of the input voltage is used as the reference. For both reference signals, the SR values increase as the direction moves away from the maximum radiation. Using the input voltage as the reference, the stretching ranges from 33.50% to 40.56%, while using its derivative as the reference, the stretching ranges only from 3.86% to 9.36%. This demonstrates the antenna's good performance in preserving the input pulse width, by keeping the stretching below 10% when using a reference signal with the same shape as the radiated electric field.

The results in time domain show that the proposed antenna is suitable to transmit/receive radiated pulses with rise time as low as 110 ps maintaining the waveform. Also, it was shown that the pulse-width SR is lower than 10% up to 30° in aperture. These properties are highly desirable for pulsed sensing applications, such as GPR or WPR, since they determine the resolution in space and the capacity of discriminating contiguous objects. The directionality of the antenna provides better performance against interference in the measurements produced by objects located behind the antenna. Directionality is desirable for sensing and also for EMI testing. The 3dB beamwidth obtained for a pulsed signal, as shown in Figure 18, is 30°.

5. Conclusions

The design and verification process for an ultra-wideband high-voltage Vivaldi antenna is presented. The antenna is implemented using a sheet composed of two aluminum layers filled with a polyester composite to reduce its weight. The operational frequency range of the designed antenna was optimized through a parametric variation on the arms geometry from 335.8 MHz to 4.2 GHz, enabling it to radiate pulses with rise time of about 110 ps. With the PLA insulator inserted between the arms of the antenna to form an insulated-coplanar-plates transmission line, it can operate at voltages of up to 12.4 kV and can provide broadband impedance matching to a standard 50 Ohm system. This capability makes the designed Vivaldi antenna suitable for applications in radar, electromagnetic compatibility (EMC), or intentional electromagnetic interference (IEMI). The antenna maintains the radiated pulse width very close to that of the driving pulse, achieving a maximum pulse width stretch ratio (SR) of 1.0936 for variations from -30° to 30° in the E-plane and H-plane. This result translates into a low level of distortion in the radiated pulse. It was shown also that the 3 dB beamwidth is 30° for a UWB pulsed signal, which is desirable for sensing and EMI testing.

Author Contributions: Conceptualization, J.J.P.; methodology, J.J.P., O.A.N.M. and H.F.G.M.; software, O.A.N.M. and H.F.G.M.; validation, J.J.P., O.A.N.M., H.F.G.M. and A.P.A.; formal analysis, J.J.P.; investigation, J.J.P., O.A.N.M. and H.F.G.M.; resources, J.J.P., O.A.N.M., H.F.G.M. and A.P.A.; data curation, J.J.P. and O.A.N.M.; writing—original draft preparation, J.J.P., O.A.N.M., H.F.G.M. and A.P.A.; writing—review and editing, J.J.P. and O.A.N.M.; visualization, A.P.A.; supervision, J.J.P.; project administration, O.A.N.M.; funding acquisition, O.A.N.M. and A.P.A. All authors have read and agreed to the published version of the manuscript.

Funding: This research was funded by the Research Directorate of Fundación Universitaria Los Libertadores, Internal Research Call No. 13 of 2025, grant number ING-0525.

Institutional Review Board Statement: Not applicable.

Data Availability Statement: The original contributions presented in the study are included in the article, further inquiries can be directed to the corresponding author.

Conflicts of Interest: The authors declare no conflicts of interest.

Abbreviations

The following abbreviations are used in this manuscript:

UWB	Ultra-Wideband
EMC	Electromagnetic Compatibility
EMI	Electromagnetic Interference
TWR	Through-Wall Radar
TSA	Tapered Slot Antenna
GPR	Ground-Penetrating Radar
RC	Reverberation Chamber
IEMI	Intentional Electromagnetic Interference
DUT	Device Under Test
AVA	Antipodal Vivaldi Antenna
SR	Pulse Width Stretch Ratio
PLA	Polylactic Acid
HFSS	High Frequency Structure Simulator
VNA	Vector Network Analyzer
HB	Hyperband
AF	Antenna Factor
VFG	Voltage Forward Gain

References

1. Yadav, R.; Malviya, L. UWB antenna and MIMO antennas with bandwidth, band-notched, and isolation properties for high-speed data rate wireless communication: A review. *International Journal of RF and Microwave Computer-Aided Engineering* **2020**, *30*, e22033, [<https://onlinelibrary.wiley.com/doi/pdf/10.1002/mmce.22033>]. <https://doi.org/https://doi.org/10.1002/mmce.22033>.
2. Ahmed Ibrahim, Jan Machac, R.S. UWB MIMO Antenna for High Speed Wireless Applications. *Applied Computational Electromagnetics Society Journal (ACES)* **2019**, *34*, 1294–1299.
3. Zakeri, H.; Azizpour, R.; Khoddami, P.; Moradi, G.; Alibakhshikenari, M.; Hwang See, C.; Denidni, T.A.; Falcone, F.; Koziel, S.; Limiti, E. Low-Cost Multiband Four-Port Phased Array Antenna for Sub-6 GHz 5G Applications With Enhanced Gain Methodology in Radio-Over-Fiber Systems Using Modulation Instability. *IEEE Access* **2024**, *12*, 117787–117799. <https://doi.org/10.1109/ACCESS.2024.3446313>.
4. Wong, K.L.; Hong, S.E.; Li, W.Y. Low-Profile Four-Port MIMO Antenna Module Based 16-Port Closely-Spaced 2×2 Module Array for 6G Upper Mid-Band Mobile Devices. *IEEE Access* **2023**, *11*, 110796–110808. <https://doi.org/10.1109/ACCESS.2023.3322730>.
5. Elmansouri, M.A.; Filipovic, D.S. Pulse Distortion and Mitigation Thereof in Spiral Antenna-Based UWB Communication Systems. *IEEE Transactions on Antennas and Propagation* **2011**, *59*, 3863–3871. <https://doi.org/10.1109/TAP.2011.2163785>.
6. Cicchetti, R.; Miozzi, E.; Testa, O. Wideband and UWB Antennas for Wireless Applications: A Comprehensive Review. *International Journal of Antennas and Propagation* **2017**, *2017*, 2390808, [<https://onlinelibrary.wiley.com/doi/pdf/10.1155/2017/2390808>]. <https://doi.org/https://doi.org/10.1155/2017/2390808>.
7. Elsheakh, D.M.; Abdallah, E.A. Compact shape of vivaldi antenna for water detection using ground penetrating radar. *Microwave and Optical Technology Letters* **2014**, *56*, 1801–1809, [<https://onlinelibrary.wiley.com/doi/pdf/10.1002/mop.28451>]. <https://doi.org/https://doi.org/10.1002/mop.28451>.

8. Sato, M.; Hamada, Y.; Feng, X.; Kong, F.N.; Zeng, Z.; Fang, G. GPR using an array antenna for landmine detection. *Near Surface Geophysics* **2004**, *2*, 7–13. [<https://onlinelibrary.wiley.com/doi/pdf/10.3997/1873-0604.2003011>]. <https://doi.org/https://doi.org/10.3997/1873-0604.2003011>.
9. Kumar, O.P.; Kumar, P.; Ali, T.; Kumar, P.; Vincent, S. Ultrawideband Antennas: Growth and Evolution. *Micromachines* **2022**, *13*. <https://doi.org/10.3390/mi13010060>.
10. Rafique, U.; Pisa, S.; Cicchetti, R.; Testa, O.; Cavagnaro, M. Ultra-Wideband Antennas for Biomedical Imaging Applications: A Survey. *Sensors* **2022**, *22*. <https://doi.org/10.3390/s22093230>.
11. Latha, T.; Ram, G.; Kumar, G.A.; Chakravarthy, M. Review on Ultra-Wideband Phased Array Antennas. *IEEE Access* **2021**, *9*, 129742–129755. <https://doi.org/10.1109/ACCESS.2021.3114344>.
12. Jamshidi-Zarmehri, H.; Akbari, A.; Labadlia, M.; Kedze, K.E.; Shaker, J.; Xiao, G.; Amaya, R.E. A Review on Through-Wall Communications: Wall Characterization, Applications, Technologies, and Prospects. *IEEE Access* **2023**, *11*, 127837–127854. <https://doi.org/10.1109/ACCESS.2023.3331743>.
13. Ghimire, J.; Choi, D.Y. Ultra-Wide Band Double-Slot Podal and Antipodal Vivaldi Antennas Feed by Compact Out-Of-Phase Power Divider Slot for Fluid Properties Determination. *Sensors* **2022**, *22*. <https://doi.org/10.3390/s22124543>.
14. D, R.S.; Azeemuddin, S. A comprehensive review of high voltage wideband and ultra-wide band antennas for IEMI applications. *Engineering Research Express* **2021**, *3*, 012001. <https://doi.org/10.1088/2631-8695/abd873>.
15. Gibson, P. The Vivaldi Aerial. In Proceedings of the 1979 9th European Microwave Conference, 1979, pp. 101–105. <https://doi.org/10.1109/EUMA.1979.332681>.
16. Bhattacharjee, A.; Bhawal, A.; Karmakar, A.; Saha, A.; Bhattacharya, D. Vivaldi antennas: a historical review and current state of art. *International Journal of Microwave and Wireless Technologies* **2021**, *13*, 833–850. <https://doi.org/10.1017/S1759078720001415>.
17. Gutierrez, S.; Pantoja, J.J.; Ruiz, E.F.; González, N.; Vega, F.; Baer, C.; Sachs, J.; Kasmi, C. Advances on the detection of Landmines and IEDs in Colombia using UWB GPR and Machine Learning Techniques. In Proceedings of the 2021 15th European Conference on Antennas and Propagation (EuCAP), 2021, pp. 1–4. <https://doi.org/10.23919/EuCAP51087.2021.9411214>.
18. Al Mesmari, A.; Pantoja, J.J.; Alvarez, J.; Banelli, A.; Bega, F.; Kasmi, C. An Unmanned Aerial Vehicle Platform for the detection of Landmines and IEDs using GPR. In Proceedings of the GlobalEM 2022, 2022, pp. 101–102.
19. García-Fernández, M.; López, Y.; Andrés, F.L.H. Airborne Multi-Channel Ground Penetrating Radar for Improvised Explosive Devices and Landmine Detection. *IEEE Access* **2020**, *8*, 165927–165943. <https://doi.org/10.1109/ACCESS.2020.3022624>.
20. Stadler, S.; Igel, J. Developing Realistic FDTD GPR Antenna Surrogates by Means of Particle Swarm Optimization. *IEEE Transactions on Antennas and Propagation* **2022**, *70*, 4259–4272. <https://doi.org/10.1109/TAP.2022.3142335>.
21. Stadler, S.; Schennen, S.; Hiller, T.; Igel, J. Realistic simulation of GPR for landmine and IED detection including antenna models, soil dispersion and heterogeneity. *Near Surface Geophysics* **2024**, *22*, 188–205, [<https://onlinelibrary.wiley.com/doi/pdf/10.1002/nsg.12282>]. <https://doi.org/https://doi.org/10.1002/nsg.12282>.
22. Pantoja, J.J.; Gutierrez, S.; Pineda, E.; Martinez, D.; Baer, C.; Vega, F. Modeling and Measurement of Complex Permittivity of Soils in UHF. *IEEE Geoscience and Remote Sensing Letters* **2020**, *17*, 1109–1113. <https://doi.org/10.1109/LGRS.2019.2942181>.
23. Marvin, A.C.; Esposito, G.; Dawson, J.F.; Flintoft, I.D.; Dawson, L.; Everard, J.A.K.; Melia, G.C.R. A wide-band hybrid antenna for use in reverberation chambers. In Proceedings of the 2013 IEEE International Symposium on Electromagnetic Compatibility, 2013, pp. 222–226. <https://doi.org/10.1109/IEMC.2013.6670413>.
24. Pantoja, J.J.; Bucheli, V.; Ross, D. Electromagnetic side-channel attack risk assessment on a practical quantum-key-distribution receiver based on multi-class classification. *EPJ Quantum Technology* **2024**, *11*. <https://doi.org/10.1140/epjqt/s40507-024-00290-6>.
25. Pantoja, J.J.; Tello, A.; Anagnostou, D.; Kirrane, J.; Stonehouse, M.; Koehler-Sidki, A.; Natrella, M.; Donaldson, R. Radiofrequency emanations of a single-photon detector. *IET Conference Proceedings* **2023**, *2023*, 55–59, [<https://digital-library.theiet.org/doi/pdf/10.1049/icp.2023.3271>]. <https://doi.org/10.1049/icp.2023.3271>.

26. Mandaris, D.; Leferink, F. Simulation and measurement of log-periodic antenna and double ridged guide horn antenna for optimised field uniformity. In Proceedings of the 2017 International Symposium on Electromagnetic Compatibility - EMC EUROPE, 2017, pp. 1–6. <https://doi.org/10.1109/EMCEurope.2017.8094814>.
27. Ivšić, B.; Friščić, F.; Dadić, M.; Muha, D. Design and Analysis of Vivaldi Antenna for Measuring Electromagnetic Compatibility. In Proceedings of the 2019 42nd International Convention on Information and Communication Technology, Electronics and Microelectronics (MIPRO), 2019, pp. 491–495. <https://doi.org/10.23919/MIPRO.2019.8756750>.
28. Dawson, J.F.; Hoad, R.; Petit, B.; Rees, T.; Robinson, M.; Bale, S.; Hough, M.; Dawson, L.; Marvin, A.; Will, I. A Lightweight, Compact, High voltage Hyperband Antenna for IEMI Testing. In Proceedings of the 2021 IEEE International Joint EMC/SI/PI and EMC Europe Symposium, 2021, pp. 154–154. <https://doi.org/10.1109/EMC/SI/PI/EMCEurope52599.2021.9559333>.
29. Dawson, J.F.; Bale, S.J.; Robinson, M.P.; Rees, T.; Petit, B.J.; Hoad, R.; Hough, M. A Pulse Antenna Suite for IEMI Testing. *IEEE Electromagnetic Compatibility Magazine* **2024**, *13*, 44–57. <https://doi.org/10.1109/MEMC.2024.10834406>.
30. Ohm, S.; Kang, E.; Lim, T.H.; Choo, H. Design of a Dual-Polarization All-Metal Vivaldi Array Antenna Using a Metal 3D Printing Method for High-Power Jamming Systems. *IEEE Access* **2023**, *11*, 35175–35181. <https://doi.org/10.1109/ACCESS.2023.3262463>.
31. Savostin, V.S.; Gevorkyan, A.V. Ultra-Wideband 10-Element Antipodal Vivaldi Antenna Array with Metallic Insert. In Proceedings of the 2023 Radiation and Scattering of Electromagnetic Waves (RSEMW), 2023, pp. 420–423. <https://doi.org/10.1109/RSEMW58451.2023.10202131>.
32. Xie, J.; Chen, C.; He, J.; Qiao, H.; Fang, X.; Qu, T.; An, J. A Bidirectional Bent Vivaldi-Connected Array With Short-Circuited Branches for UWB Pulse Radiation. *IEEE Transactions on Antennas and Propagation* **2024**, *72*, 9177–9187. <https://doi.org/10.1109/TAP.2024.3454962>.
33. Peng, L.; Xie, J.Y.; Li, X.F.; Jiang, X. Front to Back Ratio Bandwidth Enhancement of Resonance Based Reflector Antenna by Using a Ring-Shape Director and Its Time-Domain Analysis. *IEEE Access* **2017**, *5*, 15318–15325. <https://doi.org/10.1109/ACCESS.2017.2734093>.
34. Çolak, S.A.; Tokan, N.T. Time-Domain Analysis of Modified Vivaldi Antennas. In *Antennas and Wave Propagation*; Pinho, P., Ed.; IntechOpen: Rijeka, 2018; chapter 3. <https://doi.org/10.5772/intechopen.74945>.
35. Amador, M.; Rouco, A.; Albuquerque, D.; Pinho, P. Overview of Vivaldi Antenna Selection for Through-Wall Radar Applications. *Sensors* **2024**, *24*. <https://doi.org/10.3390/s24206536>.
36. Lee, D.; Raman, S.; Augustine, R. Design and Investigation on Antipodal Vivaldi Antenna Emitting a Pulse-Like Waveform for Imaging Close-Range Objects. *IEEE Access* **2024**, *12*, 135642–135650. <https://doi.org/10.1109/ACCESS.2024.3432853>.
37. Schwarzbeck. *Broadband TEM Horn Antenna*, 2021. Rev. A.
38. Arthur, P.; Kromer, M.; Harter, M. Low Frequency Edge-Slot Vivaldi Antenna for Ground Penetrating Radar Applications. In Proceedings of the 2024 25th International Microwave and Radar Conference (MIKON), 2024, pp. 160–162. <https://doi.org/10.23919/MIKON60251.2024.10633921>.
39. Riyanti, K.P.K.; Setijadi, E.; Hendranto, G.; Nurhayati, N. Optimizing Vivaldi Antenna Performance: Feeding Strategies for Broadband GPR Bandwidth Expansion. In Proceedings of the 2024 IEEE Asia-Pacific Conference on Applied Electromagnetics (APACE), 2024, pp. 270–273. <https://doi.org/10.1109/APACE62360.2024.10877408>.
40. De, S.; Kundu, S. A Planar E Shaped Antipodal Vivaldi Antenna with Elliptical Slots for GPR Application. In Proceedings of the 2024 Second International Conference on Microwave, Antenna and Communication (MAC), 2024, pp. 1–4. <https://doi.org/10.1109/MAC61551.2024.10837144>.
41. Sharma, A.; Goel, K.; Prajapati, J.; Upadhyay, M.D. S- Band GPR using Vivaldi for Object Detection. In Proceedings of the 2024 IEEE International Conference for Women in Innovation, Technology & Entrepreneurship (ICWITE), 2024, pp. 675–679. <https://doi.org/10.1109/ICWITE59797.2024.10502716>.
42. Ranjan, P.; Raj, R.; Prakash, T. Suspended Elliptical Slot-Based High Gain Antenna for GPR Application. In Proceedings of the 2024 IEEE International Conference on Interdisciplinary Approaches in Technology and Management for Social Innovation (IATMSI), 2024, Vol. 2, pp. 1–4. <https://doi.org/10.1109/IATMSI60426.2024.10502950>.

43. Wu, J.; Ma, J.; Shi, B.; Mo, K.S.; Peng, L. Design of an Ultra-Wideband Low-Profile Directional Bowtie Antenna for Ground-Penetrating Radars. In Proceedings of the 2024 International Conference on Microwave and Millimeter Wave Technology (ICMMT), 2024, Vol. 1, pp. 1–3. <https://doi.org/10.1109/ICMMT61774.2024.10671735>.
44. Matsepe, L.; Steyn, W.; Grootboom, L. UWB Slot Bow-tie Antenna for FMCW GPR Applications. In Proceedings of the 2024 IEEE-APS Topical Conference on Antennas and Propagation in Wireless Communications (APWC), 2024, pp. 91–94. <https://doi.org/10.1109/APWC61918.2024.10701753>.
45. Ali, M.U.; Abdulrazak, L.F.; Iqbal, J.; Illahi, U.; Kiani, G.I.; Khan, R.A.; Elmannai, H. Design of an optimized low-profile UWB rectangular dielectric resonator antenna with moon-shaped ground for 5G – millimeter wave applications. *AEU - International Journal of Electronics and Communications* **2025**, *200*, 155903. <https://doi.org/https://doi.org/10.1016/j.aeue.2025.155903>.
46. Mohamed, H.A.; Aboulalaa, M. A low profile super UWB- MIMO antenna with d-shaped for satellite communications, 5G and beyond applications. *Scientific Reports* **2025**, *15*. <https://doi.org/10.1038/s41598-025-96017-3>.
47. Awan, W.A.; Abbas, A.; Choi, D.; Sufian, M.A.; Hussain, N.; Kim, N. Precision Enhancement in EMC Measurements: Optimizing Multi-Layer Lens for Horn Antenna Applications. In Proceedings of the 2024 International Symposium on Antennas and Propagation (ISAP), 2024, pp. 1–2. <https://doi.org/10.1109/ISAP62502.2024.10846519>.
48. Kubo, T.; Ishida, T.; Harima, K.; Gotoh, K. Radiation Characteristics of TEM Horn and Broadband Sleeve Antennas Used for Near-Field Radiated Immunity Test. In Proceedings of the 2024 IEEE Joint International Symposium on Electromagnetic Compatibility, Signal & Power Integrity: EMC Japan / Asia-Pacific International Symposium on Electromagnetic Compatibility (EMC Japan/APEMC Okinawa), 2024, pp. 607–608. <https://doi.org/10.23919/EMCJapan/APEMCOkinaw58965.2024.10585147>.
49. Sabath, F.; Mokole, E.; Samaddar, S. Definition and Classification of Ultra-Wideband Signals and Devices. *The Radio Science Bulletin* **2005**, pp. 12–26.
50. Farr, E.G.; Baum, C.E.; Buchenauer, C.J., Impulse Radiating Antennas, Part II. In *Ultra-Wideband, Short-Pulse Electromagnetics 2*; Carin, L.; Felsen, L.B., Eds.; Springer US: Boston, MA, 1995; pp. 159–170. https://doi.org/10.1007/978-1-4899-1394-4_18.
51. Yang, Y.Y.; Chu, Q.X.; Zheng, Z.A. Time Domain Characteristics of Band-Notched Ultrawideband Antenna. *IEEE Transactions on Antennas and Propagation* **2009**, *57*, 3426–3430. <https://doi.org/10.1109/TAP.2009.2028708>.

Disclaimer/Publisher’s Note: The statements, opinions and data contained in all publications are solely those of the individual author(s) and contributor(s) and not of MDPI and/or the editor(s). MDPI and/or the editor(s) disclaim responsibility for any injury to people or property resulting from any ideas, methods, instructions or products referred to in the content.